

Soft Ellipsoid Model for Gaussian Polymer Chains

Frank Eurich and Philipp Maass

Fachbereich Physik, Universität Konstanz, 78457 Konstanz, Germany

(Dated: November 1, 2018)

A soft ellipsoid model for Gaussian polymer chains is studied, following an idea proposed by Murat and Kremer [J. Chem. Phys. **108**, 4340 (1998)]. In this model chain molecules are mapped onto ellipsoids with certain shapes, and to each shape a monomer density is assigned. In the first part of the work, the probabilities for the shapes and the associated monomer densities are studied in detail for Gaussian chains. Both quantities are expressed in terms of simple approximate formulae. The free energy of a system composed of many ellipsoids is given by an intramolecular part accounting for the internal degrees of freedom and an intermolecular part following from pair interactions between the monomer densities. Structural and kinetic properties of both homogeneous systems and binary mixtures are subsequently studied by Monte-Carlo simulations. It is shown that the model provides a powerful phenomenological approach for investigating polymeric systems on semi-macroscopic time and length scales.

PACS numbers:

I. INTRODUCTION

For many applications it is important to understand polymer dynamics on semi-macroscopic time scales corresponding to configurational changes of polymer chains on lengths scales comparable with or larger than the radius of gyration \bar{R}_G . A problem of active current research in nano-technology, for example, is the tailoring of thin polymer films on surfaces [1, 2]. Spontaneous phase separation processes of incompatible polymer blends may be used to translate a chemical pattern on the surface (as e.g. produced by the micro-contact printing technique) into a pattern of varying polymer compositions [3].

Numerical investigation of such problems by means of molecular dynamics simulations of semi-microscopic bead-spring models is not feasible. An overall configurational change of an entangled polymer chain composed of typically $N = 10^3$ monomers takes a time of order $N^4\tau_v \approx 1\text{s}$, where $\tau_v \approx 1\text{ps}$ is a characteristic time for vibrational atomic motions. Changes of the morphology (e.g. significant changes of phase domains during demixing of incompatible polymer blends) then take several minutes, and this is far beyond accessible time scales in computer simulations.

To overcome this problem, one needs to study coarse-grained models. For describing spontaneous phase separation processes in polymer blends the Cahn-Hilliard equation is often used. In more complex situations involving hydrodynamic or elastic interactions, generalized time-dependent Ginzburg-Landau equations may be employed. Exact analytical treatments based on these equations are possible for the linear short-time regime and can become rather rich for thin films [4]. On the other hand, the exploration of the large-scale dynamics by numerical means is hard even within Ginzburg-Landau type treatments [5]. Nevertheless, numerous theoretical studies have been carried out in the past, in particular for investigating the behavior in confined geometries (for a recent review on this subject, see [6]).

An alternative way to describe polymer dynamics on semi-macroscopic time scales was suggested by Murat and Kremer [7]. They proposed a model, in which each polymer is described by an ellipsoid that can change its shape, position and orientation. The probability for a particular conformation follows from an intramolecular free energy functional. A continuous monomer distribution is assigned to each ellipsoid for a given conformation. The ellipsoids can penetrate each other and their interaction energy results from a pair potential. If the pair potential is given by a delta function, the interaction energy between two ellipsoids is proportional to the overlap integral of the respective monomer densities times an interaction parameter $\hat{\epsilon}$ [7]. A nice feature of the ellipsoid model is that the input parameters (cf. Sec. III) can be determined from more microscopic models appropriate to describe the polymer system on short time scales. In fact, in their original work Murat and Kremer considered a bead spring model as a starting point and showed how the kinetics can be explored on long time scales by employing the associated ellipsoid model.

In the present work we will present a simpler ansatz by considering Gaussian chain molecules as underlying entities. We will show that the associated “Gaussian ellipsoid model” (GEM) provides a powerful phenomenological approach for describing the long-time kinetics of interacting macromolecular systems. Moreover, Gaussian chains serve as a reference system for more realistic microscopic “input models”. Compared to these, the GEM has the following advantage: By including self-interactions of the ellipsoids (see Sec. IV), single ellipsoids show Flory type behavior, $\bar{R}_G \sim N^{3/5}$, while in dense systems with monomer concentration c larger than the overlap concentration c_* they exhibit a random walk type behavior, $\bar{R}_G \sim N^{1/2}$. In contrast to the bead spring model considered in [7], the $\bar{R}_G \sim N^{1/2}$ scaling in dense systems is obtained without an appropriate tuning of the interaction parameter $\hat{\epsilon}$ with the chain length N . In fact, we will show that the GEM obeys the well-known

scaling relation $\bar{R}_G(c, N) \sim N^{3/5} f(cN^{4/5})$ describing the dependence of \bar{R}_G on the polymerization degree N and monomer concentration c [8]. In this way the GEM allows one to study diffusive dynamics on large length scales, while accounting for the essential physical properties of polymeric systems.

From a technical point of view, we will show that the input quantities for the GEM can be described by explicit approximate formulae (valid for $N \gtrsim 30$). This allows us to calculate the overlap integrals of monomer densities analytically, thus speeding up the simulation considerably. In addition, the explicit form of the input quantities is helpful for employing the GEM in applications and may allow for analytical calculations in the future.

II. SOFT ELLIPSOID MODEL

The basic idea of the soft-ellipsoid-model is to map one polymer onto one soft particle, that is to do an additional coarse-graining of a microscopic model for polymers. *Soft* means, that one ellipsoid can overlap strongly with another. With respect to the setup of the model outlined in this section, and the definitions and notations involved, we follow closely the work of Murat and Kremer [7].

Given a polymer with $(N+1)$ monomers at positions $\mathbf{y}^{(k)}$ in a laboratory fixed coordinate system, $k = 0, \dots, N$, the associated ellipsoid has the center of mass $\mathbf{r} = \sum_{k=0}^N \mathbf{y}^{(k)} / (N+1)$ and its spatial extension is determined by the eigenvalues $\mathbf{S} = (S_1, S_2, S_3)$ of the radius of gyration tensor

$$S_{\alpha\beta} = \frac{1}{N+1} \sum_{k=0}^N (y_{\alpha}^{(k)} - r_{\alpha})(y_{\beta}^{(k)} - r_{\beta}), \quad (1)$$

where $y_{\alpha}^{(k)}$ is the α 'th component of $\mathbf{y}^{(k)}$. Throughout this paper we denote spatial indices by Greek letters and particle indices by Latin letters. The orientation of the associated ellipsoid in space is given by the orientation of the principal axis of $S_{\alpha\beta}$. Denoting the corresponding rotation matrix by \mathcal{R} , the transformation from coordinates \mathbf{y} of the laboratory fixed coordinate system to coordinates \mathbf{x} of the ellipsoid's coordinate system is

$$\mathbf{x} = \mathcal{R}(\mathbf{y} - \mathbf{r}). \quad (2)$$

Without loss of generality we choose

$$S_1 \geq S_2 \geq S_3, \quad (3)$$

that means we order the eigenvalues so that the first coordinate in the ellipsoid's coordinate system always refers to the largest axis, while the third coordinate refers to the smallest axis.

Finally, a function $\varrho(\mathbf{x}; \mathbf{S})$ is assigned to each ellipsoid in its coordinate system, which specifies the mean

monomer density of the polymer for given eigenvalues \mathbf{S} . This means, that two ellipsoids i, j with $\mathbf{S}_i = \mathbf{S}_j$ have monomer densities $\varrho(\mathbf{x}; \mathbf{S}_i)$, $\varrho(\mathbf{x}; \mathbf{S}_j)$ that can be transformed into each other by a spatial rotation. In the laboratory fixed coordinate system the monomer density $\varrho'_i(\mathbf{y})$ of polymer i is

$$\varrho'_i(\mathbf{y}) = \varrho(\mathcal{R}_i(\mathbf{y} - \mathbf{r}_i); \mathbf{S}_i). \quad (4)$$

The probability $P(\mathbf{S})$ for a polymer to have eigenvalues \mathbf{S} and the conditional monomer density $\varrho(\mathbf{x}; \mathbf{S})$ are the input quantities for the soft-ellipsoid-model. They have to be determined from a microscopic model and their form for the GEM (Gaussian chains) is discussed in Sec. III.

The free energy functional of an ensemble of M soft particles in a volume V is divided into an intramolecular part, which accounts for the possible internal configurations, and an intermolecular part, which describes the interaction between the polymers,

$$F = F_{\text{intra}} + F_{\text{inter}}. \quad (5)$$

The intramolecular part is given by the probability $P(\mathbf{S})$

$$F_{\text{intra}} = \sum_{i=1}^M F_{\text{intra}}^{(i)} = -k_B T \sum_{i=1}^M \ln P(\mathbf{S}_i), \quad (6)$$

where k_B is the Boltzmann constant and T is the temperature. The intermolecular part is given by

$$F_{\text{inter}} = \frac{1}{2} \sum_{i=1}^M \sum_{j \neq i} F_{\text{inter}}^{(ij)} + \left(\frac{1}{2} \sum_{i=1}^M F_{\text{inter}}^{(ii)} \right), \quad (7)$$

$$F_{\text{inter}}^{(ij)} = \int d^3 y \int d^3 z v(\mathbf{y}, \mathbf{z}) \varrho'_i(\mathbf{y}) \varrho'_j(\mathbf{z}), \quad (8)$$

We wrote “ $(j \neq i)$ ” in eq. (7), since one may or may not include self-interaction terms. The effective pair potential $v(\mathbf{y}, \mathbf{z})$ between two monomers can include indirect contributions mediated by solvent molecules. For the most simple choice accounting for excluded volume effects [9], $v(\mathbf{y}, \mathbf{z}) = \hat{\epsilon} b^3 \delta(\mathbf{y} - \mathbf{z})$ with $\hat{\epsilon}$ and b^3 being a “contact energy” and a “contact volume”, respectively, the interaction is given by the overlap integral of the monomer densities,

$$F_{\text{inter}}^{(ij)} = \hat{\epsilon} b^3 \int d^3 y \varrho'_i(\mathbf{y}) \varrho'_j(\mathbf{y}). \quad (9)$$

Equations (5–7,9) fix the thermodynamics of the model.

Generalizations to polymer mixtures are straightforward [7]. In a binary polymer blend we have two types of polymers A and B . For simplicity we will assume that both types have the same polymerization degree, $N_A = N_B = N$, and that a polymer of each type interacts with a polymer of the same type with an interaction $\hat{\epsilon}_{AA} = \hat{\epsilon}_{BB} = \hat{\epsilon}$, while polymers of different types interact with $\hat{\epsilon}_{AB} = \hat{\epsilon}(1 + \delta)$ (see Sec. V).

To summarize, the external parameters defining the thermodynamic state of a homogenous system are the

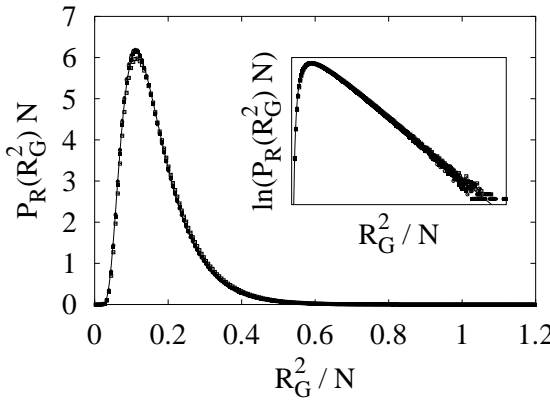


FIG. 1: Numerical results of the scaled probability function $P_R(R_G^2)$ for $N = 30(\square)$, $100(\blacksquare)$, $300(\circ)$ and $1000(\bullet)$. The approximate function $P_R(R_G^2)$ defined in the text (cf. eq. (13) and Tab. I) is drawn as a straight line. The inset shows the same data in semi-logarithmic form to prove the validity in the range of very small and very large R_G^2 .

polymerization degree N , the overall monomer concentration $c = (N+1)M/V$, and the reduced interaction strength $\epsilon \equiv \hat{\epsilon}/k_B T$. In a binary blend we in addition have the mismatch interaction δ and the fraction f_A (or concentration c_A) of A polymers.

For describing kinetic properties we implement a discrete time Monte-Carlo algorithm involving three different types of moves of a randomly chosen ellipsoid [7]: (i) A translation, where the center of mass is displaced by a random vector $\Delta\mathbf{r}$, the components of which are drawn from a uniform distribution in the interval $[-\Delta r_{\max}/2, \Delta r_{\max}/2]$; (ii) A rotation of the ellipsoid with equal probability in the steradian 4π ; (iii) A change of the ellipsoid's size, where a triplet of random numbers ΔS_α uniformly distributed in the interval $[\max(-\Delta S_{\max,\alpha}/2, -S_\alpha), S_{\max,\alpha}/2]$ is added to the eigenvalues \mathbf{S} . We restricted the changes ΔS_α to values that result only in positive S_α . Moreover, for a move according to rule (iii) it is possible that the order of the principal axes changes because of condition (3), which requires a simultaneous update of the orientation of the ellipsoid. All possible moves are attempted with the same probability and we define one Monte-Carlo step (MCS) as $3M$ trials to change the state of an ellipsoid.

We note that the dynamics are purely diffusive and neglect advective processes due to hydrodynamic flows. Moreover, the dynamics do not capture entanglement effects, which are important on time scales smaller than the disengagement time τ_D needed for a polymer to diffuse over a distance of order \bar{R}_G [9]. As a consequence, when adjusting the Monte-Carlo time step to real experimental time scales, one should take care that the dependence of τ_D on N will generally be different in the simulations and the real system.

III. GAUSSIAN ELLIPSOID MODEL (GEM)

The Gaussian chain is one of the best examined models for polymer chains. In this model the distribution of bond vectors $\Delta\mathbf{y}$ between Kuhn segments is given by

$$p(\Delta\mathbf{y}) = \sqrt{\frac{3}{2\pi b^2}} \exp\left(-\frac{3\Delta\mathbf{y}^2}{2b^2}\right), \quad (10)$$

where for simplicity we have identified the root mean square bond length b with the parameter specifying the contact volume in eq. (9). We define b as our length unit, i.e. $b \equiv 1$.

In the following we discuss the input quantities $P(\mathbf{S}, N)$ and $\varrho(\mathbf{x}; \mathbf{S}, N)$. For clarity we have now explicitly marked the dependence on N , but we take the freedom to suppress the argument N , wherever it seems to be appropriate. Explicit approximate formulae are determined for the input quantities based on Monte Carlo simulations, as well as asymptotic expansions and numerical results published in earlier work (see below). The simulations are conducted following the procedure described in [10]. Averages were performed over typically 10^7 different chain conformations.

A. Probability distribution $P(\mathbf{S})$

The exact analytical form of the distribution function $P(\mathbf{S}, N)$ for Gaussian chains is rather complicated. It can be presented in terms of multiple integrals [11], but an exact calculation from the respective formulae is very cumbersome from the numerical point of view. Useful explicit expressions are available only in the limit of large eigenvalues S_α [11, 12]. To obtain a convenient formula for practical computations, we first consider the simpler distribution function $P_R(R_G^2, N)$ of the squared radius of gyration

$$R_G^2 = \text{tr } S_{\alpha\beta} = S_1 + S_2 + S_3, \quad (11)$$

which can be expressed in terms of a single integral [13]. For large $N \rightarrow \infty$, $P_R(R_G^2, N)$ obeys the random walk scaling

$$P_R(R_G^2, N) \sim N^{-1} \tilde{P}_R(R_G^2/N), \quad \int_0^\infty du \tilde{P}_R(u) = 1. \quad (12)$$

The scaling function $\tilde{P}_R(u)$ behaves as $\tilde{P}_R(u) \sim u^{\nu_0} \exp(-C_0/u)$ for $u \rightarrow 0$ and $\tilde{P}_R(u) \sim u^{\nu_\infty} \exp(-C_\infty u)$

TABLE I: Parameter defining $P_R(R_G^2)$ in eq. (13)

n_R	1.0
a_R	0.08020
d_R	1.842
$K_0(2d_R)$	0.015923

for $u \rightarrow \infty$ [14, 15] with C_0 , C_∞ , ν_0 , and ν_∞ being constants. Note that the first moment of $\tilde{P}_R(u)$ must equal $1/6$ to obtain the well known result $R_G \equiv \langle R_G^2 \rangle^{1/2} \sim (N/6)^{1/2}$ in the limit of large N .

In this section, $\langle \dots \rangle$ denotes an average over an ensemble of Gaussian chains, while in Secs. IV, V it will also be used with respect to an ensemble of interacting ellipsoids. From the context it will be clear, what kind of average is meant.

Since the exponential terms dominate the behavior of $\tilde{P}_R(u)$ for small and large u we make the ansatz

$$\tilde{P}_R(u) \approx \frac{u^{-n_R} (a_R d_R)^{n_R-1}}{2 K_{n_R-1}(2 d_R)} \exp\left(-\frac{u}{a_R} - d_R^2 \frac{a_R}{u}\right), \quad (13)$$

where $K_{n_R-1}(\cdot)$ denotes the modified Bessel function of (n_R-1) th order accounting for proper normalization. For simplicity we restrict n_R to half-integers, but it is not supposed to equal $-\nu_0$ or $-\nu_\infty$. Since the form of the maximum turns out to depend sensitively on n_R , we determined n_R by a least square fit of (13) to the Monte Carlo data in the region given by the full width at half maximum. After determining $n_R = 1$ by this procedure, we calculated the constants a_R and d_R from the first two moments of $\tilde{P}_R(u)$ (see Appendix A and Tab. I).

Fig. 1 shows that the scaling (12) is well obeyed for $N \gtrsim 30$ [16] and that eq. (13) provides an excellent approximation to the simulated data. Moreover, higher moments $\langle R_G^{2m} \rangle$, $m = 2, 3, \dots$ calculated by using eq. (13) deviate by less than one per cent from the exact result (see Appendix A).

To find a useful approximate formula for $P(\mathbf{S}, N)$, we first consider the distributions

$$P_\alpha(S_\alpha, N) = \int d^2 S_\beta P(\mathbf{S}, N), \quad \beta \neq \alpha, \quad (14)$$

of the single eigenvalues S_α , $\alpha = 1, 2, 3$. In view of eq. (11) these can be expected to behave similar to $P_R(R_G^2, N)$. Using the random walk scaling for large N , we write $P_\alpha(S_\alpha, N) \sim N^{-1} \tilde{P}_\alpha(S_\alpha/N)$, $\int_0^\infty du \tilde{P}_\alpha(u) = 1$, with $\tilde{P}_\alpha(\cdot)$ as in eq. (13), except for the fact that the parameters n_R , a_R , and d_R are replaced by n_α , a_α , and d_α . These parameters have been determined analogous to the procedure described above (for details see Appendix A) and they are listed in Tab. II. Again, there is an excellent agreement between these functions and the simulated data, see Fig. 2.

TABLE II: Parameter defining $P_\alpha(S_\alpha)$ in eq. (15)

S_α	S_1	S_2	S_3
n_α	$1/2$	$5/2$	4
a_α	0.08065	0.01813	0.006031
d_α	1.096	1.998	2.684
$K_{n_\alpha-1}(2d_\alpha)$	0.094551	0.0144146	0.0052767

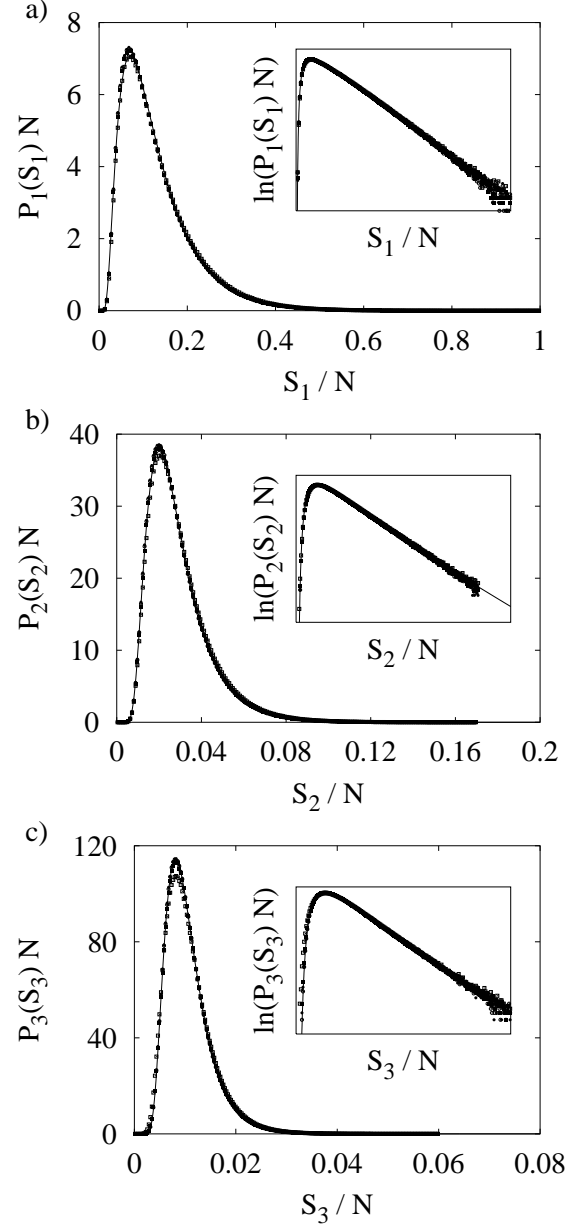


FIG. 2: Comparison of Monte-Carlo results for the scaled probability functions $P_\alpha(S_\alpha)$ for $N = 30(\square)$, $100(\blacksquare)$, $300(\circ)$ and $1000(\bullet)$ with the approximate formulae defined in eq. (15) and Tab. II. The insets show the respective data in semi-logarithmic form again.

Next, in order to obtain the combined probability density $P(\mathbf{S}, N)$, we neglect correlations among the S_α , and write

$$P(\mathbf{S}, N) = \prod_\alpha P_\alpha(S_\alpha, N) = \prod_\alpha \frac{1}{N} \tilde{P}_\alpha\left(\frac{S_\alpha}{N}\right) \quad (15)$$

$$= \prod_\alpha \frac{S_\alpha^{-n_\alpha} (a_\alpha d_\alpha N)^{n_\alpha-1}}{2 K_{n_\alpha-1}(2 d_\alpha)} \exp\left(-\frac{S_\alpha}{a_\alpha N} - d_\alpha^2 \frac{a_\alpha N}{S_\alpha}\right).$$

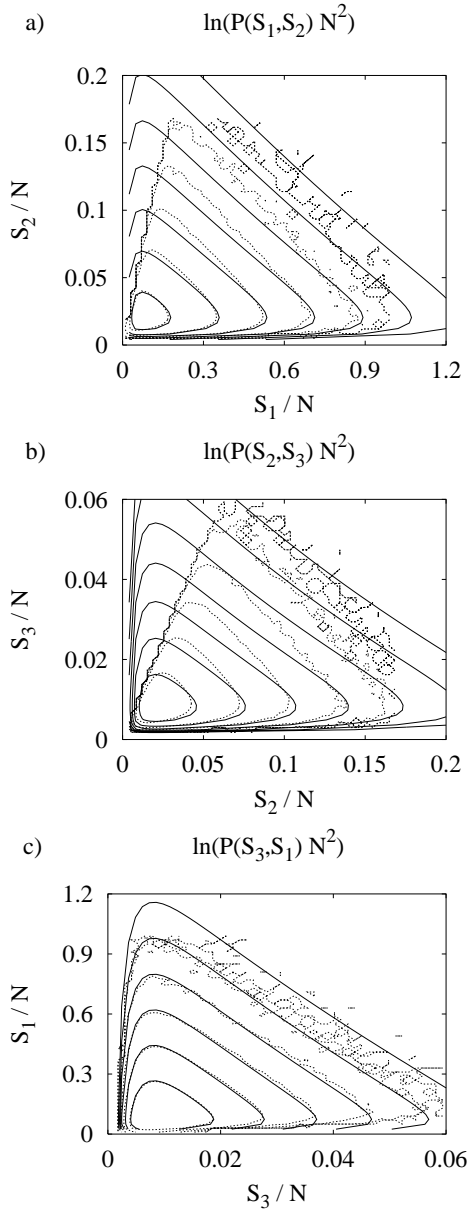


FIG. 3: Scaled contour plots showing the comparison of $\ln(P_\alpha(S_\alpha)P_\beta(S_\beta)N^2)$ (straight lines) with numerical data of $\ln P(S_\alpha, S_\beta)$ (dashed lines). The isolines are drawn at function values of 10^n , where n is an arbitrary integer number. The agreement of the separation ansatz eq. (15) with the numerical data is quite good especially in the region of large values, which have the highest statistical weight. However the separation ansatz neglects condition eq.(3). For large values of S_α the Monte-Carlo data become noisy due to insufficient statistics.

A useful test of the accuracy of eq. (15) is to check whether the correlation coefficients

$$\gamma_{\alpha\beta}^{(S)} \equiv \frac{\langle S_\alpha S_\beta \rangle - \langle S_\alpha \rangle \langle S_\beta \rangle}{\langle S_\alpha S_\beta \rangle}, \quad \alpha \neq \beta. \quad (16)$$

are much smaller than one. The results summarized in Tab. III show that all $\gamma_{\alpha\beta}^{(S)}$ are less than 6%. We also checked whether the asphericity [17]

$$\langle A \rangle = \frac{\langle R_G^2 \rangle - 3\langle S_1 S_2 + S_1 S_3 + S_2 S_3 \rangle}{\langle R_G^2 \rangle} \quad (17)$$

of the ellipsoids is significantly changed compared to the true value. From the simulations we find $\langle A \rangle \cong 0.527$, while from eq. (15) it follows $\langle A \rangle = 0.542$, which amounts to a relative error of about 3%.

A more sensitive test is the direct comparison of the combined probability density

$$P(S_\alpha, S_\beta) = \int_0^\infty dS_\gamma P(\mathbf{S}), \quad \gamma \neq \alpha, \beta \quad (18)$$

with $P_\alpha(S_\alpha)P_\beta(S_\beta)$. As shown in Fig. 3, the agreement between the ansatz (15) and the true behavior obtained from the simulations remains good, except for the regions where $P(S_\alpha, S_\beta)$ becomes extremely small. We plotted the logarithm of $P(S_\alpha, S_\beta)$ in Fig. 3, since we are interested in determining $F_{\text{intra}} \propto \ln P(\mathbf{S})$. The main restriction of (15) is that it does not obey the condition (3), i.e. $P(\mathbf{S}) = 0$ for $S_2, S_3 < S_1$ and $S_3 < S_2$. However, this poses no severe problem, because the difference in the three scales $\langle S_1 \rangle : \langle S_2 \rangle : \langle S_3 \rangle = 12.07 : 2.717 : 1$, cf. eg. Tab. IV, ensures that the location of the maximum of $P(\mathbf{S})$ is well separated from the region, where eq. (15) breaks down. Due to the exponential decrease $P_\alpha \propto \exp(-C_\alpha/S_\alpha)$ for small S_α , P is very small in the region, where it should be exactly zero.

B. Monomer density $\varrho(\mathbf{x}; \mathbf{S})$

For $\varrho(\mathbf{x}; \mathbf{S}, N)$ no exact analytical expression is available. Since $\varrho(\mathbf{x}; \mathbf{S}, N)$ is a function of many variables, various simplifications are necessary to allow for an efficient computation of the interaction terms in eq. (9). Murat and Kremer [7] proposed a self-similar monomer distribution ($R_\alpha = S_\alpha^{1/2}$),

$$\varrho(\mathbf{x}; \mathbf{S}, N) = \frac{N+1}{\prod_\alpha R_\alpha} \tilde{\varrho}(\mathbf{x}/\mathbf{R}), \quad (19)$$

where we introduced the short-hand notation $\tilde{\varrho}(\mathbf{x}/\mathbf{R}) \equiv \tilde{\varrho}(x_1/R_1, x_2/R_2, x_3/R_3)$. In contrast to [7], we included

TABLE III: Results for the correlation coefficients to test ansatz eq.(15).

$\langle \langle S_1 S_2 \rangle - \langle S_1 \rangle \langle S_2 \rangle \rangle / \langle S_1 S_2 \rangle$	0.054
$\langle \langle S_2 S_3 \rangle - \langle S_2 \rangle \langle S_3 \rangle \rangle / \langle S_2 S_3 \rangle$	0.059
$\langle \langle S_3 S_1 \rangle - \langle S_3 \rangle \langle S_1 \rangle \rangle / \langle S_3 S_1 \rangle$	0.017

the factor $[(N+1)/\prod_\alpha R_\alpha]$ in eq. (19) due to the normalization

$$\int d^3x \varrho(\mathbf{x}; \mathbf{S}, N) = N+1. \quad (20)$$

While the self-similarity assumption seems to be plausible, we will next show that it is not strictly valid. To this end we consider the function $[\prod_\alpha R_\alpha] \varrho(\mathbf{x}; \mathbf{S}, N)/(N+1)$ in terms of the scaled variable $\mathbf{u} \equiv \mathbf{x}/\mathbf{R}$, i.e. we consider

$$\hat{\varrho}(\mathbf{u}; \mathbf{S}, N) \equiv \frac{\prod R_\alpha}{N+1} \varrho(R_1 u_1, R_2 u_2, R_3 u_3; \mathbf{S}, N). \quad (21)$$

If the scaling (19) would hold true, this function would equal $\hat{\rho}(\mathbf{u})$, and hence any averaging over regions in \mathbf{S} -space would leave it invariant. In particular we define

$$\hat{\varrho}_{\alpha\beta}(u_\alpha; S_\beta, N) \equiv \int_{-\infty}^{\infty} \prod_{\mu \neq \alpha} du_\mu \int_0^\infty \prod_{\nu \neq \beta} dS_\nu P(\mathbf{S}, N) \hat{\varrho}(\mathbf{u}; \mathbf{S}, N) \quad (22)$$

that means the scaled monomer density with respect to one principal axis α under the condition that one arbitrary eigenvalue corresponding to the axis β is given. These are nine different functions, and the Monte-Carlo results for some of them are shown in Fig. 4 for $N=1000$. For other $N \gtrsim 30$ we find almost exactly the same functions, that means the scaling with N is well obeyed. In order to obtain the functions displayed in the figure, we divided the S_α -axis in eight different intervals, delimited at positions $S_\beta^{(1)} \dots S_\beta^{(9)}$, $S_\beta^{(1)} = 0$, $S_\beta^{(9)} = \infty$, each of them having the same statistical weight 1/8, i.e.

$$\int_{S_\beta^{(i)}}^{S_\beta^{(i+1)}} dS_\beta P_\beta(S_\beta) = \frac{1}{8}, \quad i = 1 \dots 8, \quad (23)$$

and averaged $\hat{\varrho}_{\alpha\beta}(u_\alpha; S_\beta)$ in each of these intervals.

Figure 4a shows the eight resulting functions for $\hat{\varrho}_{11}(u_1; S_1, N)$. By contrast to the self-similarity assumption, the curves differ significantly from each other. They

TABLE IV: Moments of the eigenvalues \mathbf{S} as determined by Monte-Carlo simulation. The table displays results for chains of length $N = 1000$ averaged over 10^7 different realizations. The data for the radius of gyration R_G are given for the sake of comparison. The deviations from the exact values for $N \rightarrow \infty$ are due to statistical errors and finite chain lengths.

$\langle R_G^2 \rangle / N$	0.16685	$\langle R_G^4 \rangle / N^2$	0.035302
$\langle S_1 \rangle / N$	0.12758	$\langle S_1^2 \rangle / N^2$	0.023009
$\langle S_2 \rangle / N$	0.028708	$\langle S_2^2 \rangle / N^2$	0.0010300
$\langle S_3 \rangle / N$	0.010568	$\langle S_3^2 \rangle / N^2$	0.00013143
$\langle S_1 S_2 \rangle / N^2$	0.0038714	$\langle S_1^3 \rangle / N^3$	0.0055805
$\langle S_2 S_3 \rangle / N^2$	0.00032239	$\langle S_2^3 \rangle / N^3$	$4.6206 \cdot 10^{-5}$
$\langle S_3 S_1 \rangle / N^2$	0.0013717	$\langle S_3^3 \rangle / N^3$	$1.9338 \cdot 10^{-6}$

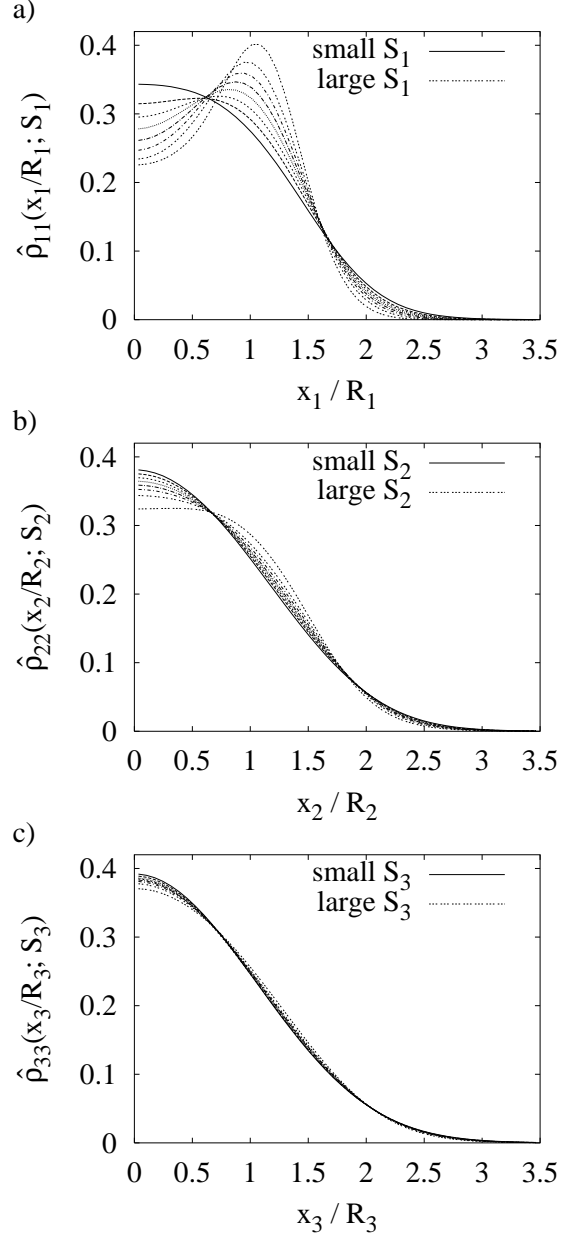


FIG. 4: One-dimensional conditional monomer density $\hat{\varrho}_{\alpha\beta}(x_\alpha/R_\alpha; S_\beta)$, scaled with $R_\alpha = \sqrt{S_\alpha}$, to demonstrate the breakdown of condition (19) in a strict sense. The curves were sampled for chain-lengths $N = 1000$.

exhibit an unimodal shape only for the smallest S_1 , while for the most likely S_1 , $\hat{\varrho}_{11}(u_1; S_1, N)$ has a bimodal shape that becomes more pronounced for larger S_1 . A similar bimodal shape for Gaussian coils has been found for the average monomer density $\bar{\varrho}(\mathbf{x}, N) \equiv \int d^3S P(\mathbf{S}) \varrho(\mathbf{x}; \mathbf{S}, N)$ by Janszen et. al. [10], and earlier for a model representing polypropylene by Theodorou and Suter [18]. For $\hat{\varrho}_{22}(u_2; S_2)$ shown in Fig. 4b, the deviations from scaling are smaller and are appreciable only for the largest S_2 , while for $\hat{\varrho}_{33}(u_3; S_3)$ in Fig. 4c the deviations are

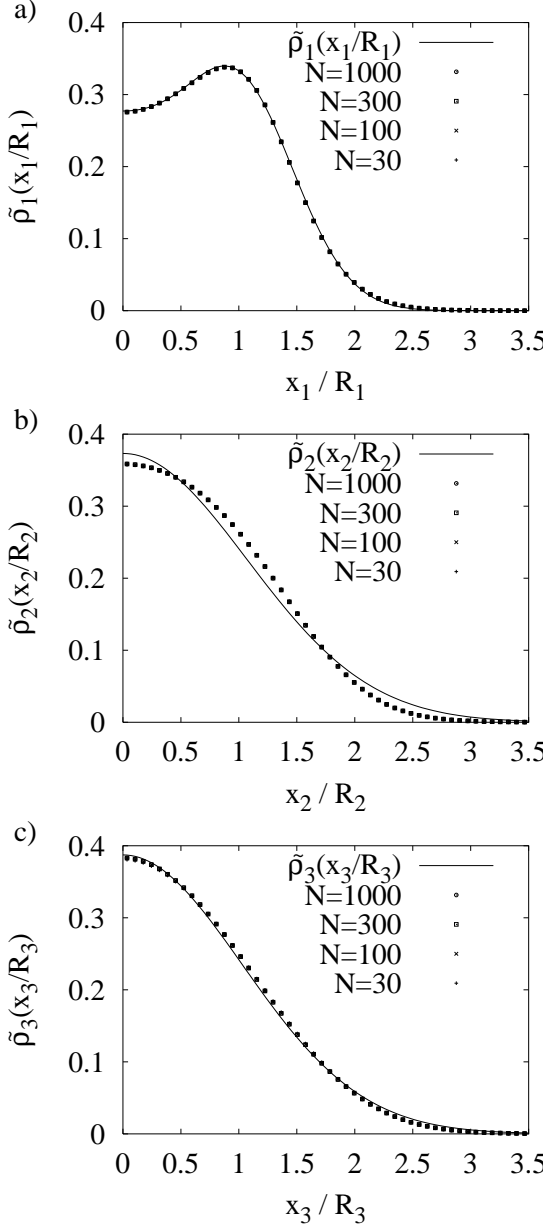


FIG. 5: Scaled one-dimensional density functions for different values of N . The straight lines denote the approximate forms given in eq. (III Ba-c).

insignificant. We also examined the six other functions and found that the deviations from scaling are small in all these cases.

In fact, knowing that the shape of $\bar{\varrho}(\mathbf{x}, N)$ in the x_1 -direction is of bimodal type, while in the x_2 -direction it is of unimodal type [10], the breakdown of the self-similarity concept is not that unexpected. If scaling would hold true, the monomer densities with respect to some fixed \mathbf{S} should correspond to the average monomer density $\bar{\varrho}(\mathbf{x}, N)$. However, if one considers the case of almost equal values of S_1 and S_2 , i.e. $S_1 \gtrsim S_2$, the

monomer densities along the x_1 - and x_2 -direction should be the same due to symmetry in contrast to the scaling prediction.

Although the self-similarity assumption is not truly valid, it can be used as a good working tool for the following reasons. The monomer densities enter the calculation of F_{inter} via integrals, cf. eq. (9). For these integrals to be correctly calculated, it is important that the size of the region, where $\varrho(\mathbf{x}, \mathbf{S}, N)$ is non-negligible, scales properly. From Fig. 4 one can see that this is indeed the case. Therefore, for our purposes it is sufficient to approximate the various functions shown in Fig. 4a-c for different S_β by their average

$$\tilde{\varrho}_\alpha(u_\alpha) = \int_0^\infty dS_\beta P_\beta(S_\beta) \hat{\varrho}_{\alpha\beta}(u_\alpha; S_\beta, N). \quad (24)$$

We marked these averaged monomer densities by a tilde, since one can view them as “effective scaling functions” representing $\bar{\varrho}(\mathbf{u})$ from eq. (19) (after integrating out the two u_μ -coordinates orthogonal to u_α). Note that we suppressed the N -argument in the definition (24), since, as already mentioned, the dependence on N predicted by eq. (19) is valid. This validity can also be inferred directly from Fig. 5, where the data for $N = 30, 100, 300$, and 1000 can not be distinguished.

The scaled monomer densities $\tilde{\varrho}_\alpha(u_\alpha)$ with $u_\alpha = x_\alpha/R_\alpha$ shown in Fig. 5 can be conveniently approximated by a superposition of Gaussians

$$\tilde{\varrho}_1(u_1) = \frac{1}{\sqrt{2\pi}\sigma_1(2+c_1)} \left[\exp\left(-\frac{(u_1 - \bar{u}_1)^2}{2\sigma_1^2}\right) + \exp\left(-\frac{(u_1 + \bar{u}_1)^2}{2\sigma_1^2}\right) + c_1 \exp\left(-\frac{u_1^2}{2\sigma_1^2}\right) \right] \quad (25)$$

$$\tilde{\varrho}_2(u_2) = \frac{1}{\sqrt{2\pi}\sigma_2} \exp\left(-\frac{u_2^2}{2\sigma_2^2}\right) \quad (26)$$

$$\tilde{\varrho}_3(u_3) = \frac{1}{\sqrt{2\pi}\sigma_3} \exp\left(-\frac{u_3^2}{2\sigma_3^2}\right) \quad (27)$$

The parameters σ_α , c_1 , and \bar{u}_1 were determined by least squares fits and are given in Tab. V. While $\tilde{\varrho}_1(u_1)$ and $\tilde{\varrho}_3(u_3)$ are quite well approximated by eqs. (25) and (27), respectively, eq. (26) does not provide such a good description. A better account for $\tilde{\varrho}_2(u_2)$ can be achieved by adding shifted Gaussian functions as in (25), and is given explicitly in appendix B. However, we decided to deal with eq. (26), because the better description increases the computation time of F_{inter} by a factor of four, but does

TABLE V: Numerical results for the constants defining $\tilde{\varrho}_\alpha(u_\alpha)$ in eqs. (III Ba-c, B1).

$\sigma_1 = 0.48920$	$c_1 = 0.64528$	$\bar{u}_1 = 0.994$
$\sigma_2 = 1.06892$		
$\sigma_3 = 1.03009$		
$\sigma'_2 = 0.748$		$\bar{u}_2 = 0.674$

not much improve the overall accuracy of $\varrho(\mathbf{x}; \mathbf{S})$. We note that the functions $\tilde{\varrho}_\alpha(u_\alpha)$ in eqs. (III Ba-c) should not be confused with the function $\bar{\varrho}(\mathbf{x}, N)$ (or its “components” after integrating out two coordinates) that has been considered earlier by Janszen et al. [10].

In order to specify the multivariate scaled density $\tilde{\varrho}(\mathbf{u})$ we employ, as for $P(\mathbf{S})$ before, a separation ansatz. This yields for $\varrho(\mathbf{x}; \mathbf{S}, N)$ from eq. (19) the final result

$$\varrho(\mathbf{x}; \mathbf{S}, N) = (N+1) \prod_{\alpha} \frac{\tilde{\varrho}(x_\alpha/R_\alpha)}{R_\alpha}, \quad (28)$$

where $\tilde{\varrho}(x_\alpha/R_\alpha)$ are taken from eqs. (III Ba-c). The separation ansatz may be used also without invoking the self-similarity assumption in order to reduce the complexity of the multivariate density $\varrho(\mathbf{x}; \mathbf{S}, N)$.

To test the validity of the separation ansatz we define for each Gaussian chain by $v_\alpha = (N+1)^{-1} \sum_{k=0}^N |x_\alpha^{(k)}|/R_\alpha$ the (scaled) mean moduli of the monomer coordinates in the principal axis system, and check whether the correlation coefficients

$$\gamma_{\alpha\beta}^{(v)} \equiv \frac{\langle v_\alpha v_\beta \rangle - \langle v_\alpha \rangle \langle v_\beta \rangle}{\langle v_\alpha v_\beta \rangle}, \quad \alpha \neq \beta, \quad (29)$$

are much smaller than one. Note that, because of the symmetry $\tilde{\varrho}_\alpha(u_\alpha) = \tilde{\varrho}_\alpha(-u_\alpha)$, we considered the moments of the moduli in (29). As shown in Tab. VI, we find $|\gamma_{\alpha\beta}^{(v)}|$ to be less than 5% in the simulations. Also, when comparing the two-variate densities

$$\tilde{\varrho}_{\alpha\beta}(u_\alpha, u_\beta) = \int_{-\infty}^{\infty} du_\gamma \tilde{\varrho}(\mathbf{u}), \quad \gamma \neq \alpha, \beta \quad (30)$$

with the two-fold products $\tilde{\varrho}_\alpha(u_\alpha) \tilde{\varrho}_\beta(u_\beta)$ in Fig. 6, a satisfactory agreement is obtained.

As an ultimate test of the separation ansatz we sampled the full three-variate scaled monomer density $\tilde{\varrho}(\mathbf{u})$ in the simulations. To this end, we subdivided the $\mathbf{u} = \mathbf{x}/\mathbf{R}$ space into small boxes of length $\Delta u_\alpha = 0.07$ and determined the mean number of monomers in each box by averaging over Gaussian chains irrespective of their \mathbf{S} . The relative error between the separation ansatz $\prod_\alpha \tilde{\varrho}_\alpha(u_\alpha)$ with $\tilde{\varrho}_\alpha(u_\alpha)$ from eqs. (III Ba-c) and the simulated $\tilde{\varrho}(\mathbf{u})$ is plotted against $\tilde{\varrho}(\mathbf{u})$ in Fig. 7 for all \mathbf{u} . We see that the relative error is confined to a narrow band of maximal 25% discrepancy except for very small $\tilde{\varrho}(\mathbf{u})$. These small $\tilde{\varrho}(\mathbf{u})$, however, are not important in the calculation of the overlap integrals in eq. (9). In principle, it would be desirable to do the same analysis also with $P(\mathbf{S})$ but

TABLE VI: Test of the ansatz eq.(28) with correlation coefficients defined in eq. (29).

$\langle \langle v_1 v_2 \rangle - \langle v_1 \rangle \langle v_2 \rangle \rangle / \langle v_1 v_2 \rangle$	-0.048
$\langle \langle v_2 v_3 \rangle - \langle v_2 \rangle \langle v_3 \rangle \rangle / \langle v_2 v_3 \rangle$	-0.027
$\langle \langle v_3 v_1 \rangle - \langle v_3 \rangle \langle v_1 \rangle \rangle / \langle v_3 v_1 \rangle$	-0.018

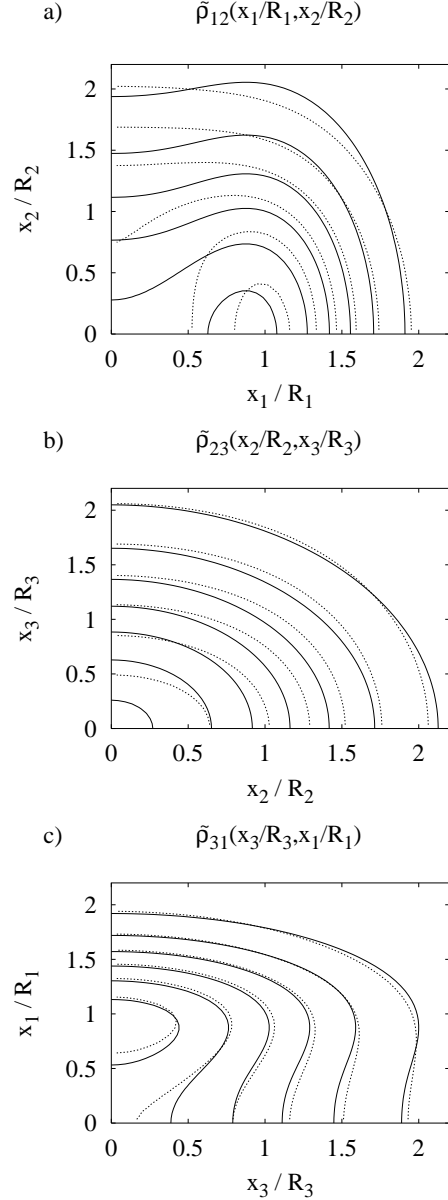


FIG. 6: Contour plots showing the comparison of $\tilde{\varrho}_\alpha(x_\alpha/R_\alpha) \tilde{\varrho}_\beta(x_\beta/R_\beta)$ (straight lines) with numerical data of $\tilde{\varrho}_{\alpha\beta}(x_\alpha/R_\alpha, x_\beta/R_\beta)$ (dashed lines). The isolines are drawn at function values, which are integer multiples of 0.02.

since one Gaussian chain generates only one realization of \mathbf{S} , it is very hard to obtain reasonable statistics in this case.

The monomer density $\varrho(\mathbf{x}, \mathbf{S}, N)$ specified in eq. (28) allows us to calculate the overlap integrals and thus F_{inter} from (9) analytically. This is explained in detail in Appendix C.

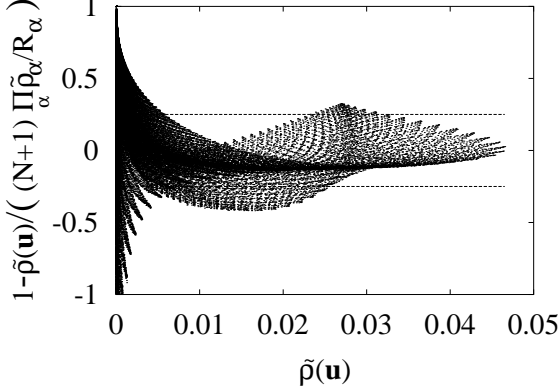


FIG. 7: The plot shows the relative error of the approximate function defined in eqs. (III B,28) when compared to 3D numerical data of $\tilde{\rho}(\mathbf{u})$ for chains of length $N = 1000$, versus the function value of $\tilde{\rho}(\mathbf{u})$. For large function values, that give the main contribution to F_{inter} , the relative error is quite small. The lines denote a 25% error interval.

C. Self-interactions

Gaussian chains are by definition non-self-interacting in contrast to real polymer chains. In order to obtain a physical model, we therefore include a self-interaction term in eq. (7), which amounts to an intermolecular part of the form

$$F_{\text{inter}} = \frac{1}{2} \sum_{i=1}^M \sum_{j \neq i} F_{\text{inter}}^{(ij)} + \frac{1}{2} \sum_{i=1}^M F_{\text{inter}}^{(ii)} \quad (31)$$

with $F_{\text{inter}}^{(ij)}$ given in eq. (9). The factors $(1/2)$ in front of both the double and simple sum in (7) arise to avoid double counting of monomer interactions.

In principle, it would be more appropriate to include the self-interaction term into the intramolecular part in eq. (6). In fact, when referring to some kind of realistic model for single polymer chains, as e.g. the bead-spring model considered by Murat and Kremer [7] this self-interaction part naturally is entailed in F_{intra} . In our case, however, interactions between monomers belonging to the same or different chains are treated *on the same footing* and we thus decided to include the self-interaction part into eq. (7). The GEM thus specified can be regarded as a Flory type model for polymer systems.

D. Remarks on the algorithm

In this section we shortly describe some details of the algorithm used throughout the rest of this work. As the Monte-Carlo method is well established [19], we just comment on some specialties in this case.

The main challenge for the setup of an optimal algorithm is to calculate the interaction term F_{inter} efficiently,

even when the calculation can be done analytically. As one polymer in a melt overlaps with many other ones, it is crucial to calculate only those interaction terms, which contribute significantly to F_{inter} . Therefore, the monomer density has to be cutoff at a certain length and we choose this cutoff to be $x_{\alpha, \text{cut}}/R_{\alpha} = 2.2$, cf. Fig. 5. The neighbors of a polymer are defined as those polymers, which interpenetrate each other within their cutoff shape. Because the ellipsoids are strongly aspherical, a simple test of the distance between the centers of mass is not efficient enough.

In order to determine whether two ellipsoids are neighbors, we introduced a grid of cells, with a spatial discretization length given approximately by the smallest significant scale, i.e. $\langle R_3 \rangle$. To every cell in the grid is assigned a list of polymers, that overlap with the cell, and conversely, to every polymer is assigned a list of cells, which it covers. Determining the neighbors j of one polymer i then is simple: One goes through the list of cells assigned to polymer i , determines all polymers j that are associated with each member of this list and finally sorts out multiple occurrences of j . For each polymer we keep a list entailing the neighbors with the respective interaction energies, and the total value of the interaction energy with the neighbors. In this way the updating of the lists after each Monte-Carlo move becomes simple. Since the calculation of F_{inter} consumes the main part of the CPU time, we parallelized this part, thus speeding up the simulation by a factor of 1.5 on a two-processor machine.

With the method described here, a fast calculation of F_{inter} is possible. However it should be noted, that the efficiency depends on the possibility to integrate the product of two densities analytically. The time for calculation depends essentially both on the overall monomer concentration c and on N (or on \bar{R}_G), because these quantities determine the average number of neighbors of one particle.

For performing one elementary step of the Monte-Carlo simulation, where we try to change either the orientation, the center of mass position or the eigenvalues \mathbf{S} of one randomly chosen ellipsoid as explained in Sec. II, we still have to specify Δr_{max} and ΔS_{max} . We choose

$$\Delta r_{\text{max}} = K_r \bar{R}_G, \quad \Delta S_{\text{max}} = K_s \langle S_{\alpha} \rangle \quad (32)$$

with $K_r = 0.25$, $K_s = 0.5$ and the $\langle S_{\alpha} \rangle$ given in Tab. IV. A trial for a change from an initial state i to a final state f is accepted with a probability p_{if} given by the Glauber rule, i.e. $p_{if} = (1/2)(1 - \tanh[(F_f - F_i)/2k_B T])$, where F_i and F_f are the free energies of the initial and final state, respectively. After each trial the time t is incremented by $\tau_0/3M$, where τ_0 is a characteristic time scale (1 MCS) that has to be adapted to the particular physical situation under consideration (see the discussion in Sec. IV below).

Unless noted otherwise, the initial conditions are as follows: The center of mass positions of the ellipsoids are randomly distributed within the simulation box. The

orientations of the ellipsoids are random, and the eigenvalues \mathbf{S}_i are drawn from the distribution $P(\mathbf{S}, N)$ for the non-interacting Gaussian chains given in eq. (14). The S_α are sorted afterwards according to rule (3). Equilibrium quantities are determined after proper thermalization.

To summarize this section, eqs. (15) and (28) together with (III B) define the input quantities for the GEM, and one has to take care of including self-interactions as explained in Sec. III C. The explicit form of the respective formulae allows for an easy reproducibility of the results to be discussed in the following sections. Despite approximate, they capture the essential features found for Gaussian chains: The normal random walk scaling with N , the strong asphericity of the chains, the bimodal form of the monomer density and its rapid decay beyond cut-off lengths that scale linearly with R_α . We note in passing that we performed also simulations for self-avoiding chains and found similar features except, of course, for the scaling with N . While it is possible to provide more accurate formulae for the input quantities by introducing more parameters, we are convinced that this is of minor importance for the study of structural properties and kinetic phenomena on semi-macroscopic length scales.

IV. HOMOGENEOUS SYSTEMS

The aim of the following section is to show that the GEM reproduces the most important semi-macroscopic properties of dilute and dense polymeric systems: The scaling properties of the radius of gyration \bar{R}_G upon N and c , the scaling behavior of the distribution $P_R(R_G^2, N)$ in a dense homogenous system of interacting ellipsoids, and the existence and scaling of the correlation hole. We partly follow the analysis proposed by Murat and Kremer [7].

As mentioned above, the free energy as given in eqs. (5–7,9) is some kind of Flory-like description of polymers. Accordingly, the gyration radius of a free ellipsoid, that only interacts with itself but not with other ellipsoids, scales as $R_G^2 \sim N^{6/5}$ [8], see Fig. 8a.

In order to obtain the dependence on ϵ also, let us redo some Flory type calculation, where for simplicity we consider soft spheres instead of soft ellipsoids. Within this approximation the monomer density from eq. (28) would become

$$\varrho_r(r; R_G) = \frac{(N+1)}{R_G^3} \tilde{\varrho}_r \left(\frac{r}{R_G} \right) \quad (33)$$

with $\tilde{\varrho}_r(u_r) = \exp(-u_r^2/2\sigma_r^2)/(2\pi\sigma_r^2)^{3/2}$, $\sigma_r^2 = 1/3$. Such a simplified form of the monomer density has been discussed already in [13]. Substituting $P_R(R_G^2)$ from eqs. (12,13) into the free energy functional $F_{\text{sph}}^{(ii)}(R_G^2) =$

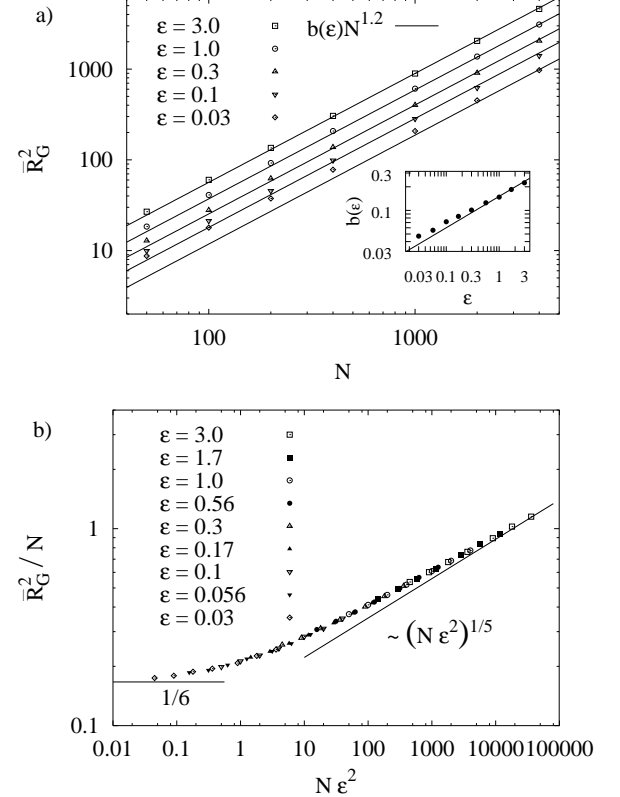


FIG. 8: a) Mean squared gyration radius of free ($c \rightarrow 0$), but self-interacting ellipsoids as a function of N , displayed for various values of the interaction strength ϵ . The Flory result $\langle R_G^2 \rangle \propto N^{6/5}$ is shown for comparison. The inset shows the dependence on ϵ . The line indicates a power law $b(\epsilon) \propto \epsilon^{2/5}$. b) Crossover scaling from Gauss to Flory type behavior.

$-k_B T \ln P_R(R_G^2) + 4\pi\hat{\epsilon} \int_0^\infty dr r^2 \varrho_r^2(r; R_G)$ we obtain

$$\frac{F_{\text{sph}}^{(ii)}(R_G^2)}{k_B T} = -\ln \left(\frac{1}{2 N K_0(2 d_R)} \right) - \ln \left(\frac{N}{R_G^2} \right) + \frac{R_G^2}{a_R N} + d_R^2 \frac{a_R N}{R_G^2} + \epsilon \frac{(N+1)^2}{32} \left(\frac{3}{\pi R_G^2} \right)^{3/2}. \quad (34)$$

The most probable value $R_{G,0}^2$ results from minimizing with respect to R_G^2 ,

$$\frac{1}{R_{G,0}^2} + \frac{1}{a_R N} - d_R^2 \frac{a_R N}{R_{G,0}^4} - \epsilon \frac{3(N+1)^2}{64 R_{G,0}^5} \left(\frac{3}{\pi} \right)^{3/2} = 0. \quad (35)$$

This equation has the asymptotic solution

$$R_{G,0}^2 \sim \left(\frac{3}{\pi} \right)^{3/5} \left(\frac{3}{64} \epsilon \right)^{2/5} N^{6/5}. \quad (36)$$

Since $\bar{R}_G^2 \sim R_{G,0}^2$, we expect $\bar{R}_G^2 \sim \epsilon^{2/5}$ in reasonable agreement with the numerical results for free, self-interacting ellipsoids, see Fig. 8a.

For small ϵ , one should recover the Gaussian behavior, i.e. we expect $\bar{R}_G^2 \sim N$ for $\epsilon \ll \epsilon_*(N)$. On the other hand, the scaling (36) must hold true for $\epsilon \gg \epsilon_*(N)$. Thus, from continuity, we find $\epsilon_*(N) \sim N^{-1/2}$. The corresponding scaling form $\bar{R}_G^2(N, \epsilon) = N f(\epsilon^2 N)$ with $f(u) \sim \text{const.}$ for $u \rightarrow 0$ and $f(u) \sim u^{1/5}$ for $u \rightarrow \infty$ is verified in Fig. 8b.

We now discuss systems composed of many interacting ellipsoids. As is well known from self-consistent field arguments [8], the Flory type scaling (36) changes to a normal random walk scaling if the monomer concentration c exceeds the overlap concentration c_* . That this is indeed the case is shown in Fig. 9. Approaching c_* from below we can write $(c_*/N)^{-1/3} \sim \bar{R}_G(N, \epsilon) \sim \epsilon^{1/5} N^{3/5}$ (for $\epsilon \gg N^{-1/2}$), i.e. $c_* \sim \epsilon^{-3/5} N^{-4/5}$, so that more generally we expect the scaling form [8]

$$\bar{R}_G^2(N, \epsilon, c) = \epsilon^{2/5} N^{6/5} f(c \epsilon^{3/5} N^{4/5}) \quad (37)$$

with $f(\lambda) \rightarrow \text{const.}$ for $\lambda \ll 1$ and $f(\lambda) \rightarrow \lambda^{-1/4}$ for $\lambda \gg 1$ to describe the crossover from dilute to dense systems. Accordingly, $\bar{R}_G^2 \sim \epsilon^{1/4} c^{-1/4} N$ for $c \epsilon^{3/5} N^{4/5} \gg 1$. To demonstrate the validity of the overall scaling predicted by eq. (37), we show in Fig. 10 as an example $\bar{R}_G^2/N^{6/5}$ as a function of $cN^{4/5}$ for a fixed value $\epsilon = 1.0$. As can be seen from the figure, the data for different c and N all collapse onto a common master curve. We note that the scaling (37) is followed only for $\epsilon \gg N^{-1/2}$. For $\epsilon \ll N^{-1/2}$ by contrast, the ellipsoids would always exhibit Gauss type behavior.

We further show in Fig. 11 that the distribution function $P_R(R_G^2, N)$ for dense systems ($c \gg c_*$) obeys the same type of scaling as for non-interacting Gaussian chains, eq. (12), $P_R(R_G^2, N) \sim N^{-1} \tilde{P}_R(R_G^2/N)$. In particular, the ansatz (13) can be used equally well for $\tilde{P}_R(u)$ up to a change of the parameters a_R , and d_R (see Tab. I and the values given in the caption of Fig. 11).

To complete our study of the static properties of dense homogeneous systems, we discuss the properties of the

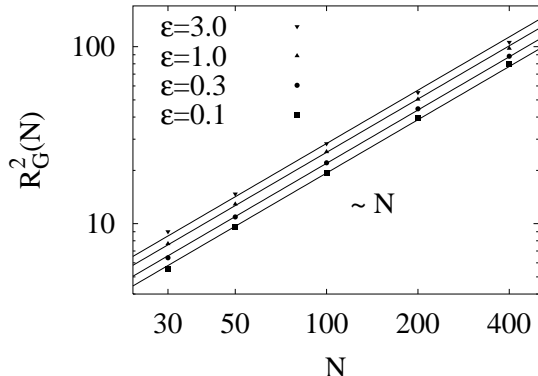


FIG. 9: Squared gyration radius R_G^2 as a function of N in a dense ($c = 0.85$) system of $M = 1000 \rightarrow 4000$ ellipsoids (double-logarithmic representation). For various values of constant ϵ a linear behavior is observed.

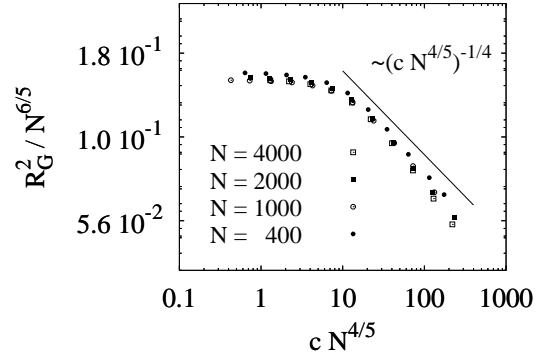


FIG. 10: Test of the scaling relation between the squared radius of gyration and the monomer concentration for various values of N and constant $\epsilon = 1.0$ (double-logarithmic representation). For small concentrations the chains are almost free and R_G^2 saturates, corresponding to Flory type behavior. In the region of high concentration the expected scaling relation is almost fulfilled.

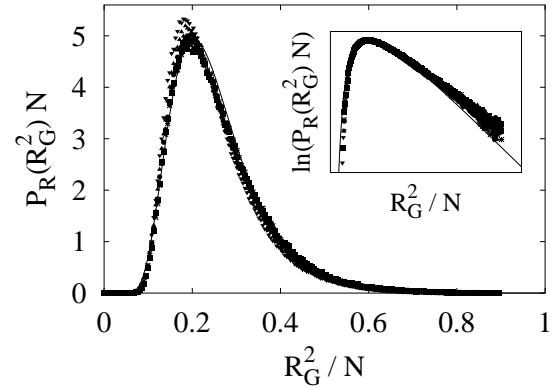


FIG. 11: Scaling behavior of the distribution function $P(R_G^2)$ in a melt system for $N = 30$ (*), 50 (■), 100 (●), 200 (▲) and 400 (▼). The straight line refers to a function of form eq. (13), but with changed parameters $a_R = 0.0665$ and $d_R = 3.52$. The inset shows the same data in semi-logarithmic representation. The external parameters are $c = 0.85$ and $\epsilon = 1.0$.

so-called correlation hole [8]. Therefore we determine the mean monomer density of all ellipsoids except the i 'th one as a function of the distance from the center of ellipsoid i ,

$$\varrho'_{\text{dist}}(r, N) = \left\langle \sum_{j \neq i} \varrho'_j(\mathbf{r} - \mathbf{r}_i, N) \right\rangle. \quad (38)$$

After performing the average in (38), this mean monomer density of “distinct ellipsoids” is equal for all i and depends on $r = |\mathbf{r}|$ only. For large $r \gtrsim \bar{R}_G$, $\varrho'_{\text{dist}}(r) \rightarrow c$, while for small $r \ll \bar{R}_G$, $\varrho'_{\text{dist}}(r)$ must be smaller than c due to the fact that ellipsoid i has been excluded from the sum in eq. (38). Since $4\pi \int_0^\infty dr r^2 [\varrho'_{\text{dist}}(r, N) - c] = -(N+1)$,

we expect a scaling $[\varrho'_{\text{dist}}(r, N) - c] \sim N^{-1/2} f(rN^{-1/2})$ for the correlation hole, in reasonable agreement with the simulated results shown in Fig. 12.

We conclude this section with some remarks on the dynamical behavior of the system. As can be seen from Fig. 13, the time-dependent mean square displacement $\langle [\mathbf{r}_i(t) - \mathbf{r}_i(0)]^2 \rangle$ of an ellipsoid exhibits normal diffusive behavior for times $t > \tau_D$, where τ_D is the disengagement time, i.e. the average time an ellipsoid needs to diffuse over a distance \bar{R}_G . The short time regime $t < \tau_D$ is not of interest here, since we do not intend to capture the complicated dynamics of polymer systems on these time scales. In particular, the diffusion coefficient $D = \lim_{t \rightarrow \infty} \langle [\mathbf{r}_i(t) - \mathbf{r}_i(0)]^2 \rangle / 6t$ will usually not exhibit the desired scaling with N , e.g. $D \sim N^{-1}$ for Rouse chains or $D \sim N^{-2}$ for entangled chains.

In fact, because D depends on Δr_{max} , and Δr_{max} is chosen to be some fraction K_r of $\bar{R}_G \sim N^{1/2}$ (see Sec. III D), the variation of D with N is influenced by the simulation procedure itself, i.e. by the value of K_r . For the choice $K_r = 0.25$ used in our simulations, D increases with N (see Fig. 13). Conceptually, this is not a crucial problem. Since the elementary time scale τ_0 in the Monte Carlo procedure (see Sec. III D) is arbitrary, we can always adjust $\tau_0 = \tau_0(N)$ in order to reproduce the desired N dependence.

Let us finally note that apart from the characteristic time scale τ_D for translational motion, there are two other characteristic time scales in the model, which refer to the change of shape and orientation of the ellipsoids. These can be identified by the decay of e.g. the correlation functions $\langle R_G^2(t) R_G^2(0) \rangle$ (shape) and $\langle \mathbf{e}_1(t) \cdot \mathbf{e}_1(0) \rangle$ (orientation), where \mathbf{e}_1 is a unit vector pointing in the direction of the first principal axis (normalized first eigenvector of $S_{\alpha\beta}$). An adjustment of these time scales to real situations is again possible by tuning K_S properly, or by restricting the rotational movements of the ellipsoids. For our choice of parameters ($K_S = 0.5$ and free

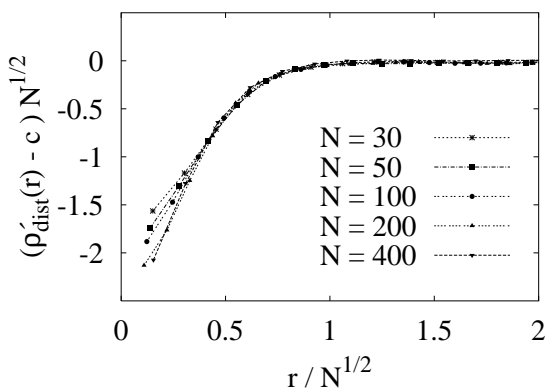


FIG. 12: Scaling behavior of the correlation hole. The monomer concentration is $c = 0.85$, the interaction parameter $\epsilon = 1.0$.

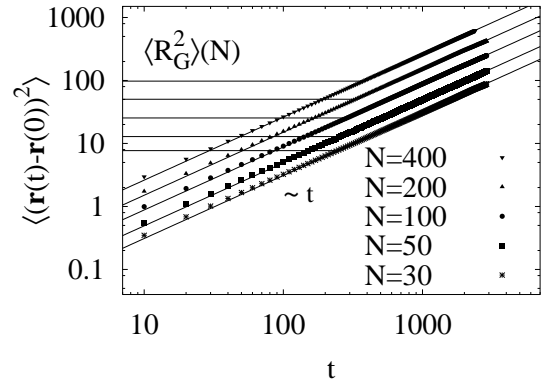


FIG. 13: Mean square displacement $\langle (\mathbf{r}(t) - \mathbf{r}(0))^2 \rangle$ as a function of time for various values of N in a dense system ($c = 0.85$, $\epsilon = 1.0$). The lines indicate a linear growth at late times. Shown for comparison is the mean squared radius of gyration $\langle R_G^2 \rangle$ in the melt for the respective N .

rotation), τ_D is the largest characteristic time scale. Accordingly, for the time scales $t \gtrsim \tau_D$ of interest here, we have not to bother about shape-sensitive or orientational correlations.

V. BINARY MIXTURES

In this section we present the results for a binary mixture of polymers. We denote the fraction of chains of type A with $f_A = M_A/M$, and the fraction of chains of the other type B with $f_B = M_B/M$. The interaction parameter is always $\epsilon = 1.0$ and we consider dense systems ($c = 0.85$).

A. Coexistence curve

First we determine the coexistence curve. The simulations are conducted for a semi-grandcanonical ensemble [7], i.e. we keep the total particle number M fixed and allowed the fractions f_A and f_B to fluctuate. To this end we allow particles to change their identity in the Monte-Carlo simulation in addition to the other possible moves. The order parameter Φ is defined by $\Phi \equiv |f_A - f_B|$. For $T < T_c$ the distribution of the order parameter $D(\Phi)$ has a maximum at a finite value $\Phi_{\text{max}} > 0$, while for $T > T_c$, $\Phi_{\text{max}} = 0$.

A convenient way to identify the phase transition in the simulation is to determine the average $\langle \Phi \rangle$. For $T \ll T_c$, $D(\Phi)$ becomes sharply peaked and $\langle \Phi \rangle \simeq \Phi_{\text{max}}$. For $T > T_c$, $\langle \Phi \rangle$ is measure of the width of $D(\Phi)$ rather than an estimate of $\Phi_{\text{max}} = 0$. However, for $T \gg T_c$ the width becomes very small and $\langle \Phi \rangle$ also. Accordingly, the critical temperature can be estimated from the region, where $\langle \Phi \rangle$ goes from large finite values to zero, see Fig. 14.

We investigated systems of $M = 4000, 3000$ and 2000 ellipsoids for chain lengths $N = 50, 100$ and 200 respectively, carrying out runs over 4000 MCS. In Fig. 14 we show $\langle |\Phi| \rangle = \langle |f_A - f_B| \rangle$ as a function of $1/N\delta = k_B T/N(\hat{\epsilon}_{AB} - \hat{\epsilon})$. The scaling of the coexistence curve with N is not perfect since $k_B T_c/\delta = A N + B$ [20, 21]. A similar behavior of the phase diagram in dependence on N has been found in simulations with explicit chains and in experiments [22].

B. Chain dimensions in a blend

An interesting physical effect in polymer blends is that the chains of the minority phase reduce their size to minimize the repulsive interaction with those of the majority phase [20, 23]. In Fig. 15 we present the results for the average squared gyration radius of the two different components A and B , divided by the pure melt value $\langle R_G^2 \rangle_0$ for $\delta = 0$. The fraction of B -particles was kept fixed at $f_B = 0.9$. As can be seen from the figure, the particles in the minority shrink much more strongly, than those in the majority. A detailed discussion of the interplay between thermodynamics and chain conformations can be found in [24].

C. Spinodal decomposition

When a polymer mixture is quenched rapidly into the mechanically unstable part of the phase diagram, demixing occurs via spontaneously growing concentration fluctuations of long wavelengths [25]. After some initial time regime, domains of the two coexisting phases form, and with increasing time these domains are expected to coarsen according to the Lifshitz-Slyozov growth law $L_D(t) \sim t^{1/3}$, where L_D denotes the average domain size.

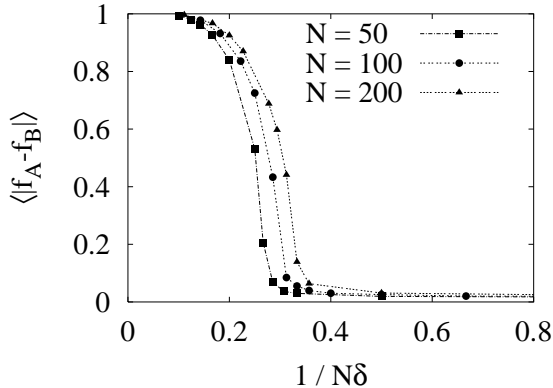


FIG. 14: The order parameter $\langle |f_A - f_B| \rangle$ plotted versus $1/N\delta = k_B T/N(\hat{\epsilon}_{AB} - \hat{\epsilon})$ for chains of length $N = 50, 100$ and 200 . The result indicates, that the coexistence curve scales almost as $1/N$.

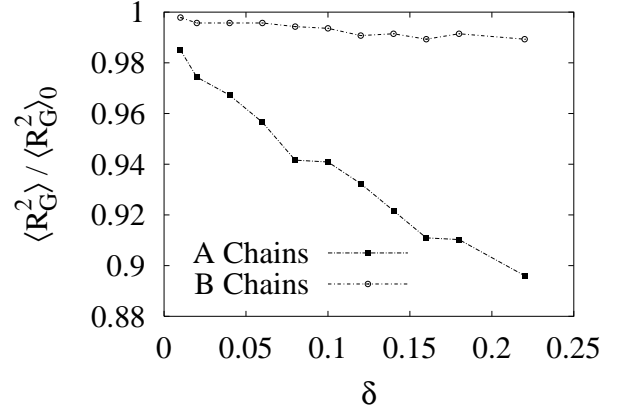


FIG. 15: Squared radius of gyration of minority ($f_A = 0.1$) and majority ($f_B = 0.9$) type chains as a function of the excess interaction parameter δ . The simulation was run for $M = 4000$ particles of length $N = 50$.

To study the spontaneous phase separation in the GEM we consider an equilibrated symmetric blend ($f_A = 0.5$) for $\delta = 0$ and increase the mismatch parameter instantaneously to $\delta = 0.2$ at time $t = 0$. The power spectrum of the concentration fluctuations is given by the intermediate scattering function

$$I(k, t) = \langle \rho_A(\mathbf{k}, t) \rho_A(-\mathbf{k}, t) \rangle - c_A^2 \delta(\mathbf{k}), \quad (39)$$

where $\rho_A(\mathbf{k}, t)$ is the Fourier transform of the total monomer density $\varrho'_A(\mathbf{y}, t) = \sum_{i=1}^{M_A} \varrho'_{A,i}(\mathbf{y}, t)$ of A -ellipsoids. The power spectrum depends on $k = |\mathbf{k}|$ only and an explicit expression of $I(k, t)$ in terms of particle positions, orientations and sizes is derived in appendix D.

The results for $I(k, t)$ are presented in Fig. 16. At early times a peak develops in $I(k, t)$, which is associated with a characteristic demixing length. For $t \leq 5000$ MCS the peak position is almost constant in time. At later times the domain pattern begins to coarsen and the peak of $I(k, t)$ shifts to smaller values of k . To quantify this coarsening process we consider the normalized first moment

$$k_1(t) = \frac{\int_0^\infty dk k I(k, t)}{\int_0^\infty dk I(k, t)} \quad (40)$$

of the intermediate scattering function, which is a measure of the inverse domain size. As shown in Fig. 17 the results point to an asymptotic approach towards the Lifshitz-Slyozov growth law $k_1(t) \sim t^{-1/3}$. We note that in more detailed microscopic models it is hard to reach the asymptotic coarsening regime due to the slow diffusion of the chain molecules (see the discussion in Sec. IV). Nevertheless, in some simulations of such models the Lifshitz-Slyozov growth law could be seen [26, 27].

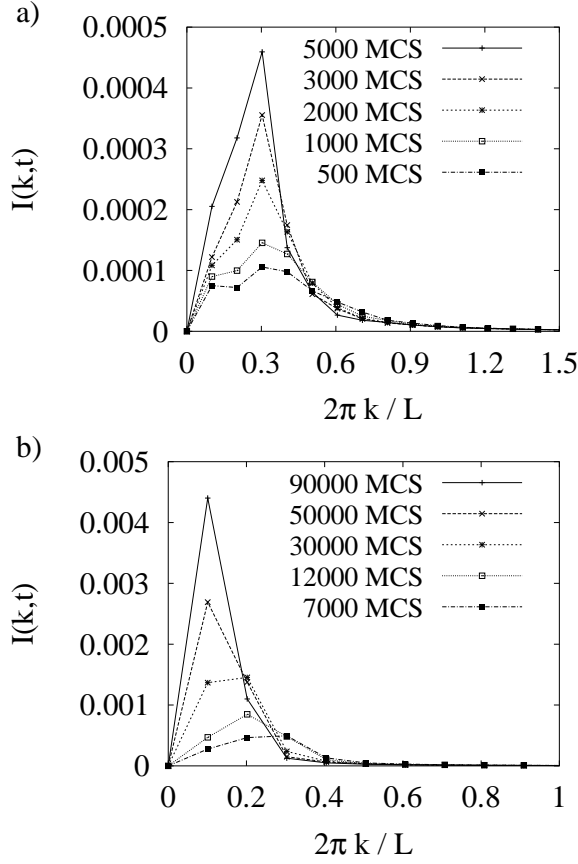


FIG. 16: Intermediate scattering function $I(k, t)$ for various times t . In the early time-regime a) the structure develops mainly at some fixed characteristic wavelength, while for later times b) the peak position of $I(k, t)$ shifts to smaller values of k demonstrating coarsening of the domain patterns. The function is only evaluated at the physically meaningful integer values of k . The data are determined for a system of $M = 4000$ particles of size $N = 50$.

VI. CONCLUDING REMARKS

In summary we have shown that the GEM provides a useful tool to study polymer systems on semi-macroscopic time and length scales. The input quantities, that are the probability $P(\mathbf{S})$ for an ellipsoid to have a shape \mathbf{S} and the mean monomer density $\varrho(\mathbf{x}; \mathbf{S})$ in the principal axis system for a given shape, were investigated in detail for Gaussian chains and expressed in terms of approximate formulae. Both homogeneous systems and binary mixtures have been simulated on the basis of these input quantities by means of a discrete Monte Carlo procedure. The results from these simulations were shown to reproduce the basic scaling relations of polymer physics.

A valuable feature of the GEM is that the interactions between the monomers of the same ellipsoid and different ellipsoids can be treated on the same footing by including self-interactions as discussed in Sec. III C. As a con-

sequence, no tuning of the interaction parameter $\hat{\epsilon}$ with N is necessary to obtain the desired Gauss type behavior in dense systems. On the other hand, an important motivation of the work of Murat and Kremer [7] for setting up the ellipsoid model was to keep a direct link to more detailed microscopic models. For such underlying models it seems that a tuning of $\hat{\epsilon}$ with N can not be avoided. However, one may ask, if it is really necessary to compare many particle simulations of the underlying microscopic model with many particle simulations of the associated ellipsoid model in order to establish the dependence of $\hat{\epsilon}$ on N , as it was done in [7]. An alternative route, dealing only with the single chain behavior of the underlying microscopic model, would be to use the Gaussian form for $P(\mathbf{S}, N)$ from eq. (15), where N is the number of Kuhn segments of the real microscopic chain with N_{mic} monomers. Then one should include self-interactions (see eq. (7)) with $\hat{\epsilon} = \hat{\epsilon}(N)$ in the associated ellipsoid model in such a manner that the true behavior of $P(\mathbf{S}, N_{\text{mic}})$ for single chains of the microscopic model is best accounted for, e.g. by requiring the first moment of $P_R(R_G^2, N)$ of the ellipsoid model with self-interaction to equal the first moment of the true $P_R(R_G^2, N_{\text{mic}})$. In this way a later tuning of $\hat{\epsilon}$ with N in the many particle simulation should no longer be necessary. The procedure seems to be particularly promising, if effective interactions of longer range are included in eq.(8), which mirror the interactions of the monomers in the underlying microscopic model.

As outlined in the Introduction, our motivation for studying the GEM stems largely from our wish to study the behavior of thin films of polymer mixtures. In this respect we regard the work for the bulk behavior outlined here as a suitable basis for further investigation. The important influence of substrate interactions on the demixing kinetics of thin films can be easily taken into account by incorporating the coupling of the monomer density to an external potential in the free energy functional. Free

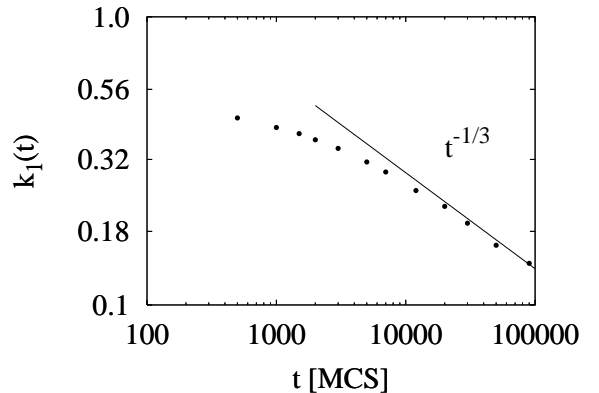


FIG. 17: Time-dependence of the first moment of the intermediate scattering function measuring the inverse domain size in double-logarithmic representation. At late stages the asymptotic Lifshitz-Slyozov behavior $k_1(t) \sim t^{-1/3}$ is reached.

surfaces can be modeled by introducing attractive interactions between the centers of the ellipsoids. These issues will be addressed in the near future.

Acknowledgments

We should like to thank W. Dieterich and J. Baschnagel for very interesting discussions and B. Rinn for supplying a parallelization package. Financial support by the Deutsche Forschungsgemeinschaft (SFB 513, Ma 1636/2-1) is gratefully acknowledged.

APPENDIX A: PARAMETERS OF THE DISTRIBUTION FUNCTIONS

The determination of the parameters is based on the fact that the moments of the heuristic functions are calculable analytically. Therefore we define the constants a_R and d_R for $P_R(R_G^2)$ in such a way, that the first two moments $\langle R_G^2 \rangle$ and $\langle R_G^4 \rangle$ are exact in the limit $N \rightarrow \infty$. With this definition and the well known [13] results $\langle R_G^2 \rangle \sim N/6$ and $\langle R_G^4 \rangle \sim 19N^2/540$ we are led to the two equations

$$a_R = \frac{1}{6} \frac{K_0(2d_R)}{d_R K_1(2d_R)}, \quad \frac{K_0(2d_R) K_2(2d_R)}{36 K_1^2(2d_R)} = \frac{19}{540}. \quad (\text{A1})$$

At this point we also give a more quantitative test of $P_R(R_G^2)$ by comparison of the higher moments of R_G^2 . The asymptotic exact result for the third moment is $\langle R_G^6 \rangle / N^3 = 631/68040 \approx 0.009274$, while we find $\langle R_G^6 \rangle / N^3 = 0.009280$. For the fourth moment the exact result $\langle R_G^8 \rangle / N^4 = 1219/408240 \approx 0.002986$ has to be compared with $\langle R_G^8 \rangle / N^4 = 0.003000$.

For $P_\alpha(S_\alpha)$ the same procedure leads to

$$\frac{\langle S_\alpha \rangle}{d_\alpha} \frac{K_{n_\alpha-1}(2d_\alpha)}{K_{n_\alpha-2}(2d_\alpha)} = a_\alpha, \quad (\text{A2})$$

$$\frac{K_{n_\alpha-3}(2d_\alpha) K_{n_\alpha-1}(2d_\alpha)}{K_{n_\alpha-2}^2(2d_\alpha)} = \frac{\langle S_\alpha^2 \rangle}{\langle S_\alpha \rangle^2}. \quad (\text{A3})$$

Since no exact analytical result for the moments $\langle S_\alpha^m \rangle$ exists to our knowledge, these quantities are determined by Monte-Carlo simulations of Gaussian chains of length $N = 1000$. The results are given in Tab. IV.

APPENDIX B: IMPROVED FORMULA FOR THE MONOMER DENSITY

For the sake of completeness, we present an improved heuristic formula for the density of the x_2 -axis:

$$\tilde{\rho}_2(u_2) = \frac{1}{\sqrt{2\pi} 2 \sigma'_2} \left[\exp\left(-\frac{(u_2 - \bar{u}_2)^2}{2 \sigma'^2_2}\right) + \exp\left(-\frac{(u_2 + \bar{u}_2)^2}{2 \sigma'^2_2}\right) \right] \quad (\text{B1})$$

Least squares fit of the constants yield $\bar{u}_2 = 0.674$ and $\sigma'_2 = 0.748$.

APPENDIX C: OVERLAP INTEGRALS

When inserting eqs.(III B,28) into eqs.(4,9) the calculation of F_{inter} reduces to a sum of nine terms of the form

$$\int_{-\infty}^{+\infty} d^3y \chi^{(1)}(\mathbf{y}) \chi^{(2)}(\mathbf{y}), \quad (\text{C1})$$

where the functions $\chi^{(j)}(\mathbf{y})$, $j = 1, 2$ are given by

$$\chi^{(j)}(\mathbf{y}) = \frac{1}{(2\pi)^{3/2} \prod_{\alpha=1}^3 \sigma_\alpha^{(j)}} \exp\left(-\frac{1}{2} \sum_\alpha \left(\frac{x_\alpha^{(j)}(\mathbf{y})}{\sigma_\alpha^{(j)}}\right)^2\right),$$

$$x_\alpha^{(j)}(\mathbf{y}) = \sum_\beta \mathcal{R}_{\alpha\beta}^{(j)}(y_\beta - w_\beta^{(j)}), \quad \sigma_\alpha^{(j)} = R_\alpha^{(j)} \sigma_\alpha. \quad (\text{C2})$$

The σ_α were defined in eq. (III B) and specified in Tab. V. Moreover, $w_\alpha^{(j)} = \pm \mathcal{R}_{1,\alpha} R_1^{(j)} u_0 + r_\alpha^{(j)}$ or $w_\alpha^{(j)} = r_\alpha^{(j)}$ depending on which of the three terms in eq. (25) contributes to $\chi^{(j)}(\mathbf{y})$. We define

$$\sigma \equiv \prod_{\alpha=1}^3 \sigma_\alpha^{(1)} \sigma_\alpha^{(2)} \quad (\text{C3})$$

$$T(\mathbf{y}) \equiv \sum_{\alpha=1}^3 \left\{ \left(\frac{x_\alpha^{(1)}(\mathbf{y})}{\sigma_\alpha^{(1)}}\right)^2 + \left(\frac{x_\alpha^{(2)}(\mathbf{y})}{\sigma_\alpha^{(2)}}\right)^2 \right\}. \quad (\text{C4})$$

With these definitions the expression (C1) reads

$$\frac{1}{(2\pi)^3 \sigma} \int_{-\infty}^{+\infty} d^3y \exp\left[-\frac{1}{2} T(\mathbf{y})\right]. \quad (\text{C5})$$

Since

$$\sum_\gamma \left(\frac{x_\gamma^{(j)}(\mathbf{y})}{\sigma_\gamma^{(j)}}\right)^2 = \sum_{\alpha,\beta} \mathcal{L}_{\alpha\beta}^{(j)} (y_\alpha y_\beta - 2w_\alpha^{(j)} y_\beta + w_\alpha^{(j)} w_\beta^{(j)}),$$

$$\mathcal{L}_{\alpha\beta}^{(j)} = \sum_\gamma \frac{\mathcal{R}_{\gamma\alpha}^{(j)} \mathcal{R}_{\gamma\beta}^{(j)}}{\left(\sigma_\gamma^{(j)}\right)^2}, \quad (\text{C6})$$

it follows that

$$T(\mathbf{y}) = \sum_{\alpha,\beta} \mathcal{A}_{\alpha\beta} y_\alpha y_\beta + \sum_\alpha B_\alpha y_\alpha + C, \quad (\text{C7})$$

where

$$\mathcal{A}_{\alpha\beta} = \mathcal{L}_{\alpha\beta}^{(1)} + \mathcal{L}_{\alpha\beta}^{(2)}, \quad (\text{C8})$$

$$B_\alpha = -2 \sum_\beta \left(\mathcal{L}_{\beta\alpha}^{(1)} w_\beta^{(1)} + \mathcal{L}_{\beta\alpha}^{(2)} w_\beta^{(2)} \right), \quad (\text{C9})$$

$$C = \sum_{\alpha,\beta} \left(\mathcal{L}_{\alpha\beta}^{(1)} w_\alpha^{(1)} w_\beta^{(1)} + \mathcal{L}_{\alpha\beta}^{(2)} w_\alpha^{(2)} w_\beta^{(2)} \right). \quad (\text{C10})$$

The quadratic form (C7) can be rewritten as

$$T(\mathbf{y}) = \sum_{\alpha, \beta} (y_\alpha - w_\alpha) \mathcal{D}_{\alpha\beta} (y_\beta - w_\beta) + E, \quad (\text{C11})$$

which yields

$$\int_{-\infty}^{+\infty} d^3y \chi^{(1)}(\mathbf{y}) \chi^{(2)}(\mathbf{y}) = \frac{\exp(-E/2)}{(2\pi)^{3/2} \sigma \sqrt{\det \mathcal{D}}}, \quad (\text{C12})$$

$$\begin{aligned} 4 \det \mathcal{D} = & 4 \mathcal{A}_{11} \mathcal{A}_{22} \mathcal{A}_{33} + \mathcal{A}_{12} \mathcal{A}_{13} \mathcal{A}_{23} \\ & - \mathcal{A}_{13}^2 \mathcal{A}_{22} - \mathcal{A}_{23}^2 \mathcal{A}_{11} - \mathcal{A}_{12}^2 \mathcal{A}_{33}, \end{aligned} \quad (\text{C13})$$

$$\begin{aligned} E = C + \frac{1}{16 \det \mathcal{D}} \Big[& B_1^2 (\mathcal{A}_{23}^2 - 4 \mathcal{A}_{22} \mathcal{A}_{33}) \\ & + B_2^2 (\mathcal{A}_{13}^2 - 4 \mathcal{A}_{11} \mathcal{A}_{33}) \\ & + B_3^2 (\mathcal{A}_{12}^2 - 4 \mathcal{A}_{11} \mathcal{A}_{33}) \\ & + 2 B_1 B_2 (2 \mathcal{A}_{12} \mathcal{A}_{33} - \mathcal{A}_{13} \mathcal{A}_{23}) \\ & + 2 B_1 B_3 (2 \mathcal{A}_{13} \mathcal{A}_{22} - \mathcal{A}_{12} \mathcal{A}_{23}) \\ & + 2 B_2 B_3 (2 \mathcal{A}_{23} \mathcal{A}_{11} - \mathcal{A}_{12} \mathcal{A}_{13}) \Big]. \end{aligned} \quad (\text{C14})$$

APPENDIX D: FOURIER TRANSFORM OF THE MONOMER DENSITY

For a total monomer density defined by

$$\varrho'(\mathbf{y}) \equiv \frac{1}{M(N+1)} \sum_{i=1}^M \varrho'_i(\mathbf{y}), \quad (\text{D1})$$

the Fourier transform is given by

$$\rho(\mathbf{k}) = \int_{-\infty}^{\infty} d^3y \varrho'(\mathbf{y}) \exp(-i \mathbf{k} \cdot \mathbf{y}). \quad (\text{D2})$$

Inserting the $\varrho'_i(\mathbf{y})$ from eq. (4) with (III B,28) yields

$$\begin{aligned} \rho(\mathbf{k}) = & \frac{1}{2 + c_1} \frac{1}{M} \sum_{i=1}^M \left\{ \int_{-\infty}^{\infty} d^3y e^{-i \mathbf{k} \cdot \mathbf{y}} \right. \\ & \times \left. \left[\chi_a^{(i)}(\mathbf{y}) + \chi_b^{(i)}(\mathbf{y}) + c_1 \chi_c^{(i)}(\mathbf{y}) \right] \right\} \end{aligned} \quad (\text{D3})$$

The three different functions $\chi_a^{(i)}(\mathbf{y})$, $\chi_b^{(i)}(\mathbf{y})$ and $\chi_c^{(i)}(\mathbf{y})$ are defined in eq. (C2), where all different kinds of $w_\alpha^{(j)}$ occur, i.e. $w_{\alpha,a}^{(j)} = +\mathcal{R}_{1,\alpha} R_1^{(j)} u_0 + r_\alpha^{(j)}$, $w_{\alpha,b}^{(j)} = -\mathcal{R}_{1,\alpha} R_1^{(j)} u_0 + r_\alpha^{(j)}$ and $w_{\alpha,c}^{(j)} = r_\alpha^{(j)}$, respectively. The integration is straightforward yielding the final result

$$\begin{aligned} \rho(\mathbf{k}) = & \frac{1}{(2 + c_1) \sigma_1 \sigma_2 \sigma_3} \frac{1}{M} \sum_{i=1}^M \frac{1}{\sqrt{S_1^{(i)} S_2^{(i)} S_3^{(i)}}} \frac{1}{\sqrt{\det \mathcal{G}^{(i)}}} \\ & \times \exp \left(-\frac{1}{2} \sum_{\alpha, \beta} k_\alpha \mathcal{G}_{\alpha\beta}^{(i)-1} k_\beta \right) \exp \left(-i \sum_\beta k_\beta r_\beta^{(i)} \right) \\ & \times \left[2 \cos \left(\sum_\beta k_\beta \mathcal{R}_{1\beta}^{(i)} R_1^{(i)} u_0 \right) + c_1 \right] \end{aligned} \quad (\text{D4})$$

Here we defined $\mathcal{G}_{\alpha\beta}^{(i)} = \sum_\gamma g_\gamma^{(i)} \mathcal{R}_{\gamma\alpha}^{(i)} \mathcal{R}_{\gamma\beta}^{(i)}$ and $g_\gamma^{(i)} = \left(\left(\sigma_1^2 S_1^{(i)} \right)^{-1}, \left(\sigma_2^2 S_2^{(i)} \right)^{-1}, \left(\sigma_3^2 S_3^{(i)} \right)^{-1} \right)$. The center of mass of the i 'th particle is denoted by $r_\beta^{(i)}$. The intermediate scattering function is then obtained by using eq. (D4) in eq. (39) for all times t (for the A ellipsoids).

[1] L. Sung, A. Karim, J. F. Douglas, and C. C. Han, Phys. Rev. Lett. **76**, 4368 (1996).

[2] F. Bruder and R. Brenn, Phys. Rev. Lett. **69**, 624 (1992).

[3] M. Böltau, S. Walheim, J. Mlynek, G. Krausch, and U. Steiner, Nature **391**, 877 (1998).

[4] H. P. Fischer, P. Maass, and W. Dieterich, Europhys. Lett. **42**, 49 (1998); *ibid.* Phys. Rev. Lett. **79**, 893 (1997).

[5] B. Kenzler, F. Eurich, P. Maass, B. Rinn, J. Schropp, E. Bohl, and W. Dieterich, Comp. Phys. Comm. (in press).

[6] K. Binder, J. Non-Equil. Thermodyn. **23**, 1 (1998).

[7] M. Murat and K. Kremer, J. Chem. Phys. **108**, 4340 (1998).

[8] P.-G. de Gennes, *Scaling Concepts in Polymer Physics* (Cornell University Press, Ithaca, New York, 1979).

[9] M. Doi and S. F. Edwards, *The Theory of Polymer Dynamics* (Oxford Science Publications, 1988).

[10] H. W. H. M. Janszen, T. A. Tervoort, and P. Cifra, Macromolecules **29**, 5678 (1996).

[11] G. Wei and B. E. Eichinger, Macromolecules **23**, 4845, (1990).

[12] B. E. Eichinger, Macromolecules **18**, 211, (1985).

[13] H. Yamakawa, *Modern Theory of Polymer Solutions* (Harper & Row, New York, 1971).

[14] M. Fixman, J. Chem. Phys. **36**, 306 (1962).

[15] W. C. Forsman and R. E. Hughes, J. Chem. Phys. **38**, 2118 (1963).

[16] We examined chains of length $N = 2 - 7$ and 10, too, and found larger deviations from scaling.

[17] J. Rudnick and G. Gaspari, J. Phys. A **19**, L191 (1986).

[18] D. N. Theodorou and U. W. Suter, Macromolecules **18**, 1206 (1985).

[19] *Monte Carlo and Molecular Dynamics Simulations in Polymer Science* edited by K. Binder (Oxford University Press, New York, 1995).

[20] K. Binder, in [19], p. 356 and references therein.

[21] H.-P. Deutsch and K. Binder, J. Phys. (France) II **3**, 1049 (1993).

[22] M. D. Gehlsen, J. H. Rosedale, F. S. Bates, C. D. Wignall, and K. Almdal, Phys. Rev. Lett. **68**, 2452 (1992).

[23] A. Sariban and K. Binder, Macromolecules **21**, 711 (1988).

[24] M. Müller, Macromolecules **31**, 9044 (1998).

[25] A. J. Bray, Adv. Phys. **43**, 357 (1994).

[26] A. Sariban and K. Binder, Macromolecules **24**, 578 (1991).

[27] G. Brown and A. Chakrabarti, Phys. Rev. E **48**, 3705 (1993).